Paper published in Applied Acoustics (2022) 109055 [accepted 30/9/22]
DOI: 10.1016/j.apacoust.2022.109055

A practical approach to modelling railway vehicle interior acoustics

Wenjing Sun[a], David J. Thompson[b,*], Zhanfei Zhang[a], Giacomo Squicciarini[b],

[a] Institute of Rail Transit, Tongji University, Shanghai 201804, P.R. China
[b] Institute of Sound and Vibration Research, University of Southampton, Southampton SO17 1BJ, United Kingdom
*: corresponding author, email: djt@isvr.soton.ac.uk

Abstract

The aim of the current work is to propose a practical approach for modelling the interior acoustics of railway vehicles by investigating the spatial decay of sound within the vehicle and its relation to the reverberation time and absorption. Measurements are presented of the longitudinal distribution of sound level inside five railway vehicles as well as the corresponding reverberation times. Both quantities are determined using an omnidirectional sound source located near one end of the vehicle. The measured sound pressure level follows a roughly linear dependence with longitudinal distance and the rate of decay is found to follow a consistent trend over all five datasets when plotted against reverberation time. To interpret these results, three different modelling approaches are considered: ray tracing, Statistical Energy Analysis, and an analytical corridor model. Ray tracing models with a simple geometry resembling the interior of a railway carriage are used to explore the dependence of the spatial decay and reverberation time on the absorption and scattering coefficients of the surfaces. For high values of scattering coefficient, the reverberation time approaches the Sabine estimate but for low values of scattering coefficient it can be up to a factor of 2.5 greater than this estimate. This implies difficulties in deducing the average absorption coefficients from the measured reverberation times. The spatial decay rates obtained from the ray tracing model do not have the same consistent dependence on reverberation time as the measured results, although the results for low values of scattering coefficient are closer to the measured trend than those for higher values. Investigation of the

Statistical Energy Analysis approach shows that it predicts a spatial decay rate that depends explicitly on length of the subsystems used in the model; consequently, the results do not converge as the model is refined. It is possible to use modified coupling loss factors based on an analytical corridor model to give a better approximation to the spatial decay. This corridor model is shown to give results that are consistent with the measurements if the average absorption is obtained from the reverberation time using a modified formula for the mean free path length, and if the cross-section area is reduced to allow for the blocking effect of the seats. This provides a practical way forward for using SEA for the interior sound in railway vehicles.

Key words: rail vehicle acoustics; reverberation time; spatial decay; scattering; statistical energy analysis

1. Introduction

As train speeds increase, the need to control the interior acoustic environment becomes more and more important. The interior of a railway vehicle is an extended acoustic volume, which is generally much longer in one direction than the other two. Sound is generally found to decay along its length so that the conventional Sabine room acoustics formulae are not applicable. Vehicle interiors vary widely; intercity carriages have relatively closely spaced seats, which are often quite absorptive, and the vehicles are often fitted with carpet; conversely, metro carriages have minimal seating and hard floor coverings. (Note: a ‘carriage’ is a passenger vehicle; the words ‘vehicle’ and ‘carriage’ are used largely interchangeably in this paper). Noise enters rail vehicles by airborne and structure-borne paths [1, 2] through the floor, walls, windows, doors, gangway etc; the sources with the largest contribution are often concentrated near the ends of the carriages [3].

To determine the distribution of sound within a vehicle, various methods can be applied. Deterministic methods such as the finite element method (FEM) may be applied at low frequencies, e.g. [4, 5], but are usually limited to frequencies below a few hundred hertz as the size of model required increases dramatically as frequency increases. Due to the approximately rectangular geometry, an analytical model of the interior may also be used to construct the low frequency interior acoustic field on the basis of simple room modes [6] but this has a similar limitation. At higher frequencies the number of structural and acoustic

modes increases dramatically, and such approaches become prohibitive. In common with room acoustics, the preferred analysis methods for frequencies above about 200 Hz are therefore ray tracing or Statistical Energy Analysis (SEA).

Forssén et al. [7] used the commercial ray tracing software ODEON to model the interior noise distribution in a 1/5 scale model vehicle interior containing seats and partial partitions for a point source at one location. Good agreement was found with measurements. Panahi and Younesian [8] also used the hybrid ray tracing and image source method in ODEON to study the interior acoustics of a railway vehicle with compartments. Reverberation times were predicted and compared with measurements. Octave band sound pressure spectra in four compartments also showed good agreement with measurements.

Yoshizawa et al. [9] applied the ray tracing method to an intercity carriage, both with and without seats fitted. Comparisons were made with measurements using a loudspeaker placed on the floor near one end of the carriage. In the absence of seats and tables, the predicted results at three positions in the aisle at a height of 1.6 m agreed well with the measurements for 500 Hz and above. However, when seats and tables were included, the agreement was less satisfactory, both in the aisle positions and at seat positions. It was believed that this was caused by the fact that only first order diffraction effects at the edges of seats, tables and luggage racks were included. To simulate running conditions, multiple sources were used on the interior surfaces with source strengths based on measured panel vibration, giving good agreement with measurements.

SEA has also been used by many authors to predict the noise inside rail vehicles. Sadri et al. [10] represented an open saloon intercity carriage with a conventional SEA model with 12 subsystems along its length and compared the spatial sound decay with detailed measurements inside the carriage for a point source near the centre. A Bayesian technique was used to update the model. Li et al. [11] divided the main interior cavity of a metro carriage into nine subsystems (with two small ones for the gangway regions) and compared the sound pressure distribution with running measurements. Various other authors have used SEA models of the vehicle interior as part of a more complete prediction of interior noise [12-14]. For example, Zhang et al. [14] included 100 interior cavity subsystems in their SEA model of a high-speed train, which comprised a total of 500 subsystems.

Within each subsystem of an SEA system, no account is taken of the variation of acoustic energy, so an acoustic volume is often divided into multiple subsystems to give an impression of the spatial variation. Fahy [15] suggested that the interior cavity of an automobile can be divided arbitrarily into subsystems, despite the fact that they do not satisfy the 'weak coupling' condition. However, he stated it may be more problematic to apply this to long cavities such as aircraft or train interiors.

Kang [16] reviewed different approaches for determining the sound attenuation in long enclosures and concluded that a geometrical reflection model (i.e. using image sources) seems practical but is limited to acoustically hard and smooth boundaries. Redmore and Flockton [17] proposed a model for the sound energy decay in corridors. Away from the direct field of the source this gave the rate of attenuation of sound level with distance (in dB/m) as

$$\Delta = \frac{10}{\ln(10)}\frac{\pi}{8}\frac{U\alpha}{S_{2D}} = 1.7\frac{U\alpha}{S_{2D}} \tag{1}$$

where S_{2D} is the cross-section area perpendicular to the axial direction, U is the perimeter length of this cross-section and α is the absorption coefficient. Sound level decays from Eq. (1) gave reasonable agreement with measurements in corridors. Redmore [18] subsequently performed measurements on scale model corridors in which the absorption could be more closely defined and found better agreement by using a constant of 1.4 in place of 1.7. Hopkins [19] gave a theoretical derivation for the sound decay by considering two-dimensional sound fields in cross-sections of the corridor and obtained

$$\Delta = \frac{10}{\ln(10)}\frac{1}{\pi}\frac{U\alpha}{S_{2D}} = 1.38\frac{U\alpha}{S_{2D}} \tag{2}$$

agreeing with Redmore's later empirical results. Redmore [18] also included a simple method to allow for reflections from the far end of the corridor, writing the sound pressure level (SPL) at a longitudinal distance x from the source in the absence of the direct field as

$$\mathrm{SPL}(x) - \mathrm{SPL}(0) = 10\log_{10}(10^{-\Delta x/10} + R10^{-\Delta(2L-x)/10}) \tag{3}$$

where L is the length of the corridor from the source and R is the (energy) reflection coefficient of the far end.

In an alternative approach, Picaut et al. [20] used a diffusion equation to predict the sound propagation in long rooms with diffusely reflecting boundaries. Their formulation depends on

a diffusion coefficient which is proportional to the mean free path length and an exchange coefficient that is related to wall absorption.

Based on Eq. (1), Craik [21] derived an equivalent coupling loss factor (CLF) for use in an SEA model of a corridor, in which it was assumed that all subsystems have the same length and the same absorption. This equivalent CLF is used to force the SEA formulation to fit the physics of the corridor problem but means that the coupling loss factor depends on the absorption. Moreover, it was noted that there can be difficulties in obtaining the correct values of absorption. This approach has been used for example by Orrenius and Enblom [22] to model a train interior.

Kohrs et al. [23] compared the sound decay inside a rail vehicle obtained with ray tracing (using ODEON) and SEA for a point source, which showed good agreement. No details were given of the input parameters used, although it is understood that the SEA model includes Craik's correction to the CLFs. Forssén et al. [7] employed a five-subsystem SEA model to predict the noise inside their 1:5 scale model railway carriage. This model comprised three passenger saloons and two intermediate vestibules, so the subdivision into subsystems was aligned with the interior partial partitions. Within each subsystem, however, the spatial decay was adjusted using Eq. (1), giving good agreement with measurements.

Jang and Hopkins [24] combined ray tracing and a general form of experimental SEA to determine coupling loss factors for use in an SEA model of a long room. The ray tracing model was used with either specular or diffuse reflections. This use of experimental SEA based on simulations allowed indirect coupling to be included between SEA subsystems that are not directly adjacent to one another. In comparison with the ray tracing results, they found that Eq. (2) can give estimates of spatial decay in an empty corridor that are in some cases too large and in others too small, depending on the absorption coefficient. They also made measurements in a corridor when it was empty and when it included staggered partial-height barriers.

The aim of the current work is to investigate the spatial decay of sound within the interior of a railway carriage and to use the results to propose a practical modelling approach. In Section 2, measurements are presented in five diverse rail vehicles based on an omnidirectional sound

source located at one end. From these, the longitudinal sound distributions and reverberation times are determined. To explore the dependence of these parameters on the absorption coefficient, ray tracing models are used in Section 3, with a simple overall geometry and dimensions resembling the interior of a railway carriage. Whereas Jang and Hopkins [24] considered the extreme cases of specular or diffuse reflections, here the effect of varying the scattering coefficient over a broad range is also investigated. Comparisons are also made with the analytical corridor model of Eq. (2). A method is proposed and evaluated in Section 4 for estimating the average absorption coefficient from reverberation time measurements. In Section 5 the implications of using the conventional SEA approach are investigated, and the use of Craik's modified coupling loss factors is introduced. The conclusions are summarised in Section 6.

2. Vehicle interior noise measurements

2.1 Summary of trains measured

Measurements have been taken inside five railway carriages, as listed in Table 1. The first (A) was a metro vehicle; it was used as a laboratory and contained several tables along the walls but had no seats fitted. The second and third were also metro vehicles, one with acoustically hard reflecting seats (B) and the other with upholstered seats (C). In each of these three vehicles, there was a wide gangway connection to the next vehicles which was open with no internal doors. The final two (D, E) were shorter saloons within intercity trains, with upholstered seats that are more closely arranged than in vehicle C.

Table 1. Details of railway vehicles in which measurements have been taken.

Vehicle	Description	Length, m	Width, m	Height, m	Source height, m	Mic. height, m
A	Metro vehicle with no seats	21.7*	2.95	2.10	1.6	1.6
B	Metro vehicle with hard seats	18.7*	2.45	2.15	0.2	1.5
C	Metro vehicle with soft seats	18.5*	2.45	2.15	0.2	1.5
D	Intercity vehicle with soft seats	12.0	3.36	1.95	0.2	1.2
E	Intercity vehicle with carpet and soft seats	7.5	2.65	1.90	1.6	1.6

*: with open gangway to next vehicle

2.2 Reverberation times

The reverberation time (in the form of T_{20}) was measured in each carriage in one-third octave bands using the interrupted noise method [25]. An omnidirectional sound source was placed at the height listed in Table 1 and close to one end of the carriage; the microphones were located at various positions along the centre of the carriage. The average reverberation time over these positions is shown in Figure 1. The metro vehicles with either no seats (A) or hard seats (B) have reverberation times which rise from moderate values at low frequencies up to values of 0.7-1.1 s between about 1 and 6.3 kHz. The intercity trains, by contrast, have reverberation times which remain around 0.2-0.3 s over almost the whole frequency range.

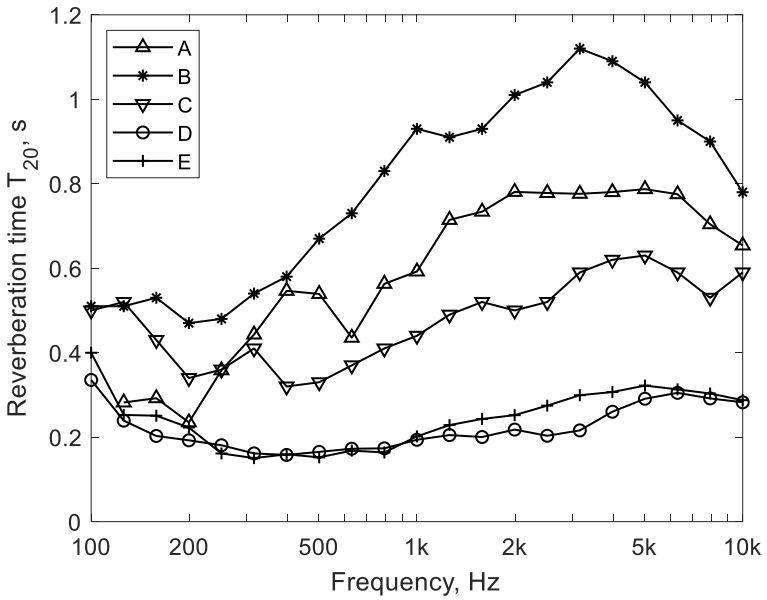

Figure 1. Reverberation times measured in five railway vehicles.

2.3 Measured decay with distance

A series of microphones were arranged within the vehicle at the heights indicated in Table 1. A typical arrangement is shown schematically in Figure 2. The microphones were spaced roughly 1 m apart and were arranged along the central aisle, or in the case of the metro vehicles, close to the centreline of the vehicle. The sound source was located close to one end and driven by a broadband random noise signal; the sound pressure spectrum was recorded at each position.

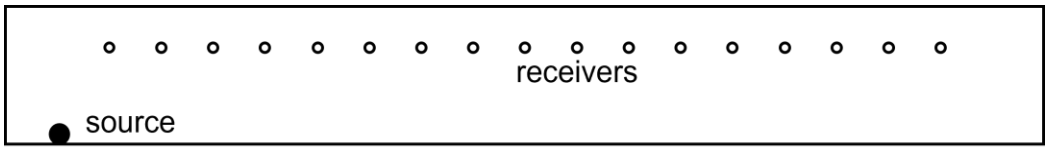

Figure 2. Schematic diagram of source and receiver locations (side view).

The variation of sound level with distance is determined in octave bands from 250 to 4000 Hz. Examples of these results are shown in Figure 3 for metro vehicle C in various frequency bands and in Figure 4 for the other vehicles in the 1000 Hz band. Sound levels are shown relative to the first measurement point in each case. Fitted curves are also shown which are obtained by a linear curve fit to all except the first and last points. As expected, the decay rate is higher in the vehicles (and frequency bands) where the reverberation time is lower.

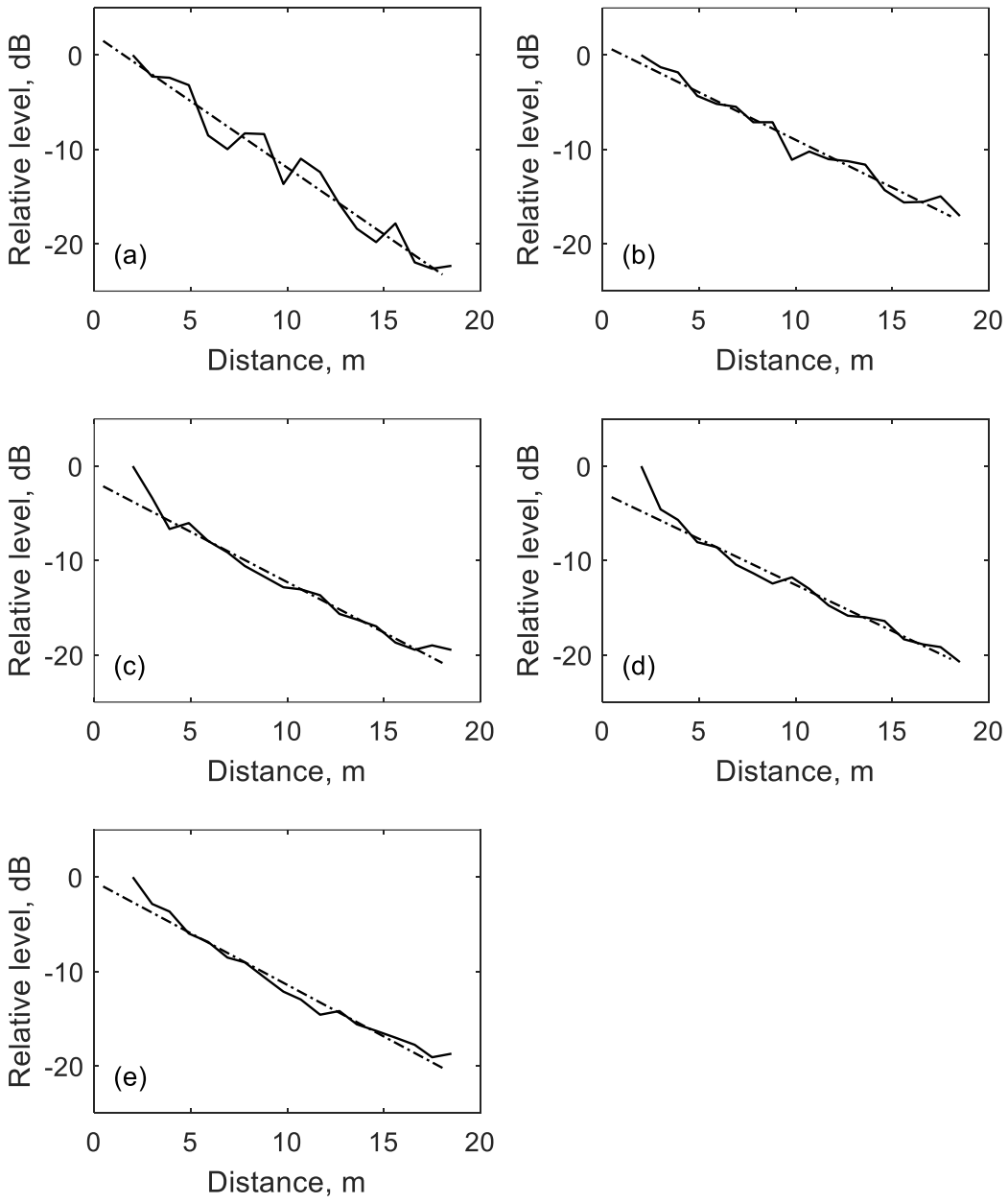

Figure 3. Sound level decay with distance in vehicle C in octave bands: (a) 250 Hz; (b) 500 Hz; (c) 1000 Hz; (d) 2000 Hz; (e) 4000 Hz.

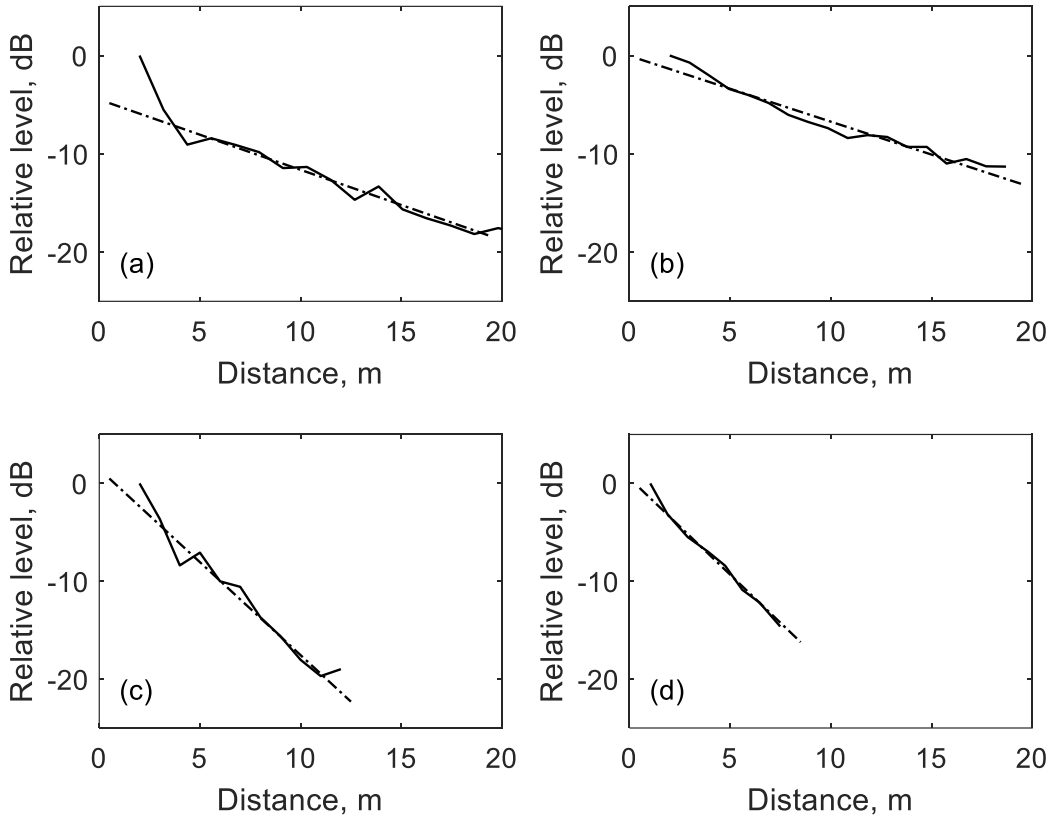

Figure 4. Sound level decay with distance in 1000 Hz octave band: (a) vehicle A; (b) vehicle B; (c) vehicle D; (d) vehicle E.

2.4 Sound spatial decay rate

The rate of spatial decay Δ in dB/m in each octave band 250-4000 Hz and in each vehicle has been obtained from the fitted curves such as those shown in Figures 3 and 4. This rate of spatial decay is plotted in Figure 5 against the corresponding average octave-band reverberation time for the five vehicles and five octave bands. A roughly linear dependence can be observed (on these log scales) as indicated by the dashed line, which is given by

$$\Delta = 0.55\, T^{-0.75} \qquad (4)$$

where T is the reverberation time.

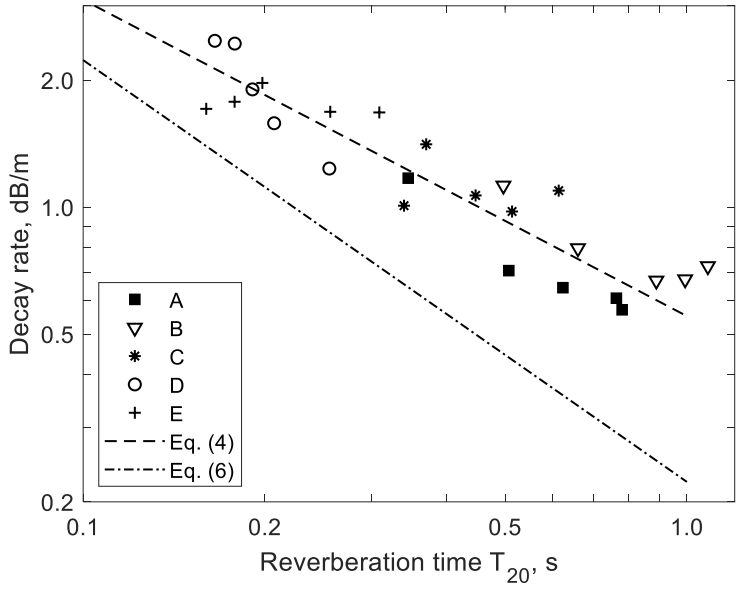

Figure 5. Spatial decay rate in octave bands 250-4000 Hz measured in the five vehicles plotted against measured reverberation time.

To apply the analytical model of Eq. (2) to the measurements, the average absorption coefficient is required. This is not known directly, but is commonly obtained from the reverberation time by using the Sabine formula

$$T = \frac{0.161V}{S\bar{\alpha}} \tag{5}$$

in which V is the room volume, S is the total room surface area and $\bar{\alpha}$ is the surface-averaged absorption coefficient. Although the sound field in a rail vehicle does not satisfy the conditions for the application of this formula (in particular, the homogeneity of acoustic energy distribution is not met), it is explored as a first attempt to determine the absorption from reverberation time, as this is commonly used in practice. As the carriage is much longer in one direction than in its cross-section, Eq. (5) can be approximated by writing $V/S \approx S_{2D}/U$, where S_{2D} is the area of the 2D cross-section and U is the perimeter length of this cross-section. Then, combining Eq. (2) and Eq. (5),

$$\Delta = \frac{10}{\ln(10)}\frac{1}{\pi}\frac{0.161}{T} = \frac{0.223}{T} \tag{6}$$

which is independent of the cross-section dimensions. This result is also shown in Figure 5. However, from these results it is clear that this estimate is too low. As will be seen in the next section, this can be explained, at least in part, by the inadequacy of the Sabine formula for such a situation.

3. Ray tracing models of a simple vehicle interior

3.1 Reverberation time

In this section, ray tracing models are introduced for a simple geometry representative of a train interior. The software CATT-Acoustic (version 9.0c/TUCT v1.1a:4.01) is used, which is based on randomized tail-corrected cone-tracing [26]. This software is used to determine source-receiver impulse responses from which sound levels and reverberation times are derived.

The model is a rectangular box of length 20 m, width 2.5 m and height 2.1 m. All surfaces are assigned the same frequency-independent absorption coefficient and scattering coefficient; eight values of absorption coefficient are considered and five values of scattering coefficient, both ranging between 0.1 and 0.7, giving 40 combinations in total. For simplicity there are no seats in the model. An omnidirectional sound source is located on the centreline at 1 m from the left-hand end and 0.2 m above the floor; receivers are located on the centreline at a height of 1.6 m and at 1 m spacing between 2 m and 19 m from the left-hand end. The arrangement is similar to that shown in Figure 2. There is no air absorption considered in the model and consequently the results obtained are independent of frequency, apart from small random variations caused by the rays used in the model and the scattering model. To minimise the influence of these variations, the average results from the 1000, 2000 and 4000 Hz octave bands are used for further analysis.

The TUCT software offers three different cone-tracing algorithms for source-receiver echograms and impulse responses. The second algorithm is used, identified as ‘Longer calculation, detailed auralization’. The number of rays/cones and length of impulse response were chosen automatically by the software: in all cases the number of primary rays was set to 12491, whereas the length of the impulse response varied from 74 ms to 1040 ms. In each case this exceeds the time taken for the sound to decay by 30 dB.

The model is used to determine the reverberation time, which is obtained using the T_{20} estimate from the impulse response. The reverberation times are shown in Figure 6 for the various values of absorption coefficient α and scattering coefficient s. For large values of the

scattering coefficient, the results correspond closely to the estimate obtained from the Sabine formula (Eq. (5)), shown as the dashed line, but for lower values of scattering coefficient the reverberation time exceeds that from the Sabine formula by up to a factor of 2.5.

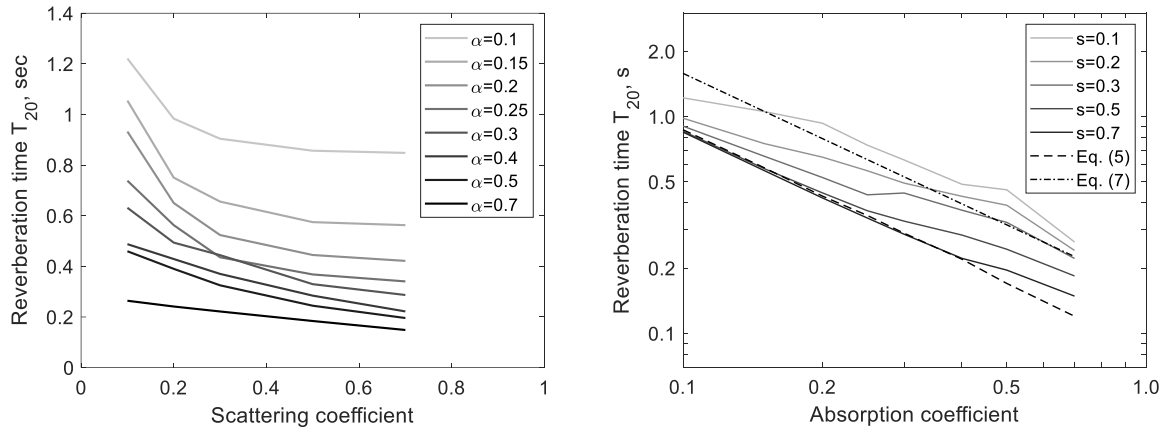

(a) (b)

Figure 6. Reverberation times obtained from the ray tracing model.

The Sabine equation, Eq. (5), corresponds to a mean free path length in a diffuse field of $4V/S$, where V is the room volume and S is the total surface area [19]. For a long room, Picaut et al. [20] found an alternative expression for the mean free path length, given by Pujolle [27], to be more appropriate. This expression gives the mean free path length as $\sqrt{S/4\pi}$, from which the reverberation time can be related to the absorption coefficient by

$$T = \frac{0.161}{4\bar{\alpha}}\sqrt{\frac{S}{4\pi}} = \frac{0.0114\sqrt{S}}{\bar{\alpha}} \qquad (7)$$

For the current geometry, this result is shown as the dash-dot line in Figure 6(b) which corresponds more closely to the ray tracing results for lower values of scattering coefficient.

3.2 Sound level variation with distance

The ray tracing models are also used to determine the sound pressure level at each position by integrating the squared impulse response. The omnidirectional sound source is assigned an arbitrary sound power level of 105 dB re 10^{-12} W in each octave band. The sound pressure level is plotted against longitudinal distance for some example cases in Figure 7. Also shown is the direct sound pressure field.

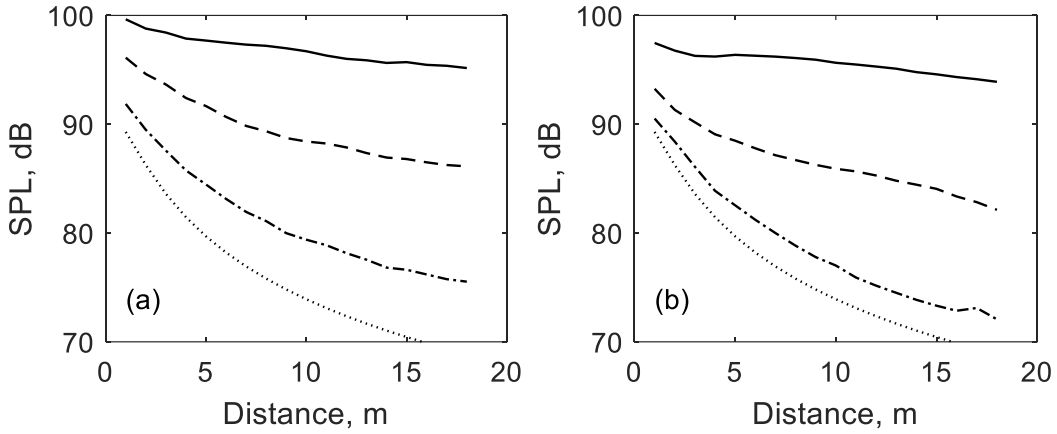

Figure 7. Sound pressure level in ray tracing model plotted as a function of longitudinal distance from the source. (a) Scattering coefficient 0.1; (b) scattering coefficient 0.7. —, $\alpha = 0.1$; – – –, $\alpha = 0.3$; – · –, $\alpha = 0.7$; ·····, direct field.

The direct sound field affects the results close to the source for higher values of absorption coefficient. The direct sound field can be subtracted from the overall mean-square pressures to give the decay in the reverberant part of the field. The corresponding results are shown in Figure 8. In most cases a more linear trend with distance is observed, although for low scattering and high absorption a nonlinear trend remains apparent.

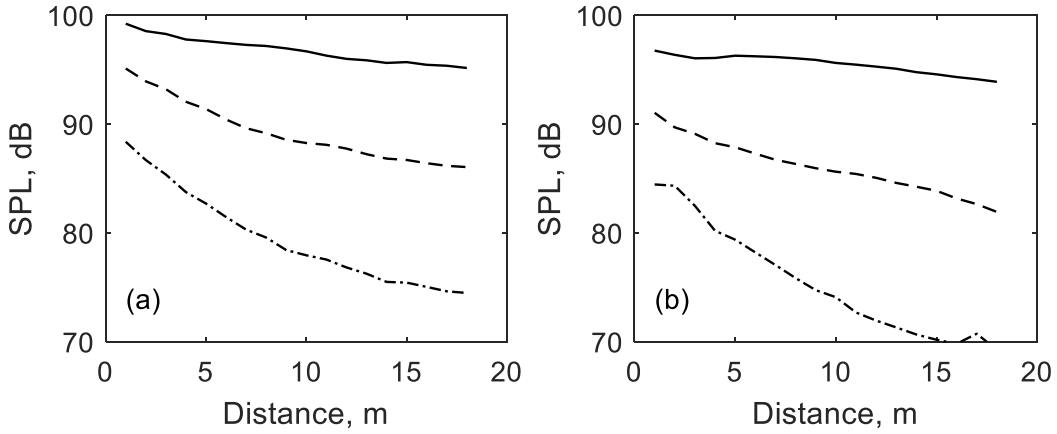

Figure 8. Sound pressure level in ray tracing model after removal of direct field, plotted as a function of longitudinal distance from the source. (a) Scattering coefficient 0.1; (b) scattering coefficient 0.7. —, $\alpha = 0.1$; – – –, $\alpha = 0.3$; – · –, $\alpha = 0.7$.

3.3 Correction for end reflections

Another potential area of influence on these results is that due to reflections from the far end of the carriage. These can be accounted for approximately by using Eq. (3) from Redmore [18]. Figure 9(a) shows the longitudinal distribution of sound pressure level for different values of α calculated using Eq. (3) combined with the decay rates from Eq. (2). The value of R is chosen to be $(1 - \alpha)$ in each case for consistency with the ray tracing model. For small values of absorption coefficient, the reflections can be seen to affect the sound level over most of the length, whereas for higher absorption values the effect is limited to regions close to the far end. By fitting a linear trend to these modified results from Figure 9(a), an apparent decay rate can be obtained; this is the decay rate that would be obtained from the curve fitting procedure if the results are 'contaminated' by the end reflections. The curve fitting is applied over distances between 2 and 9 m for consistency with the following section. In Figure 9(b) this apparent decay rate is compared with the actual decay rate Δ in the absence of end reflections, i.e. the value entered in Eq. (3).

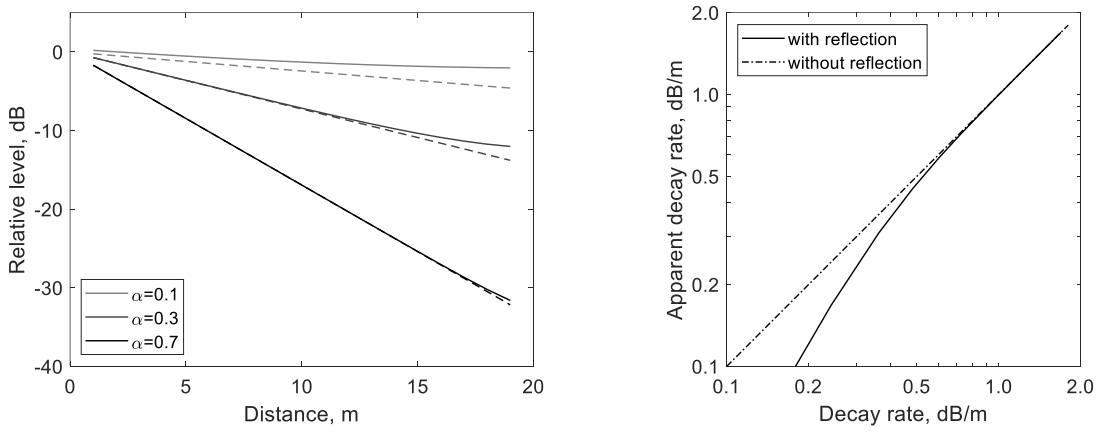

(a) (b)

Figure 9. Effect of end reflections in 20 m long vehicle. (a) Sound pressure level variation according to Eq. (3) with (solid line) and without (dash line) end reflections; (b) comparison of apparent decay rate with actual decay rate without end reflections.

Although the end reflections have a significant effect on results for decay rates less than about 0.5 dB/m (Figure 9(b)), it may be noted that the decay rates from the measurement results of Figure 5 are all greater than 0.5 dB/m. For this level of decay rate, the effect of end reflections is likely to be small. Moreover, for vehicles A-C there are no end doors; the

gangway was open to the next carriage so there are no end reflections for these cases. Consequently, no correction has been applied to the measured results.

3.4 Spatial decay

Linear trend lines have been fitted to results such as those in Figure 8 over distances *x* from 2 to 9 m. (This region is expected to be most relevant in modelling a rail vehicle interior as, beyond this region, sources at the other end of the vehicle will become predominant). The decay rates obtained are plotted against the absorption coefficient in Figure 10(a). Especially for large values of absorption coefficient, there is little variation between the results in Figure 10(a) for different values of scattering coefficient. The result from the analytical corridor model, Eq. (2), is also shown. This latter result generally gives slightly higher estimates of the decay rate than the ray tracing results but with a similar trend.

Figure 10(b) shows the results after including a correction for end reflections, based on Figure 9. This correction mainly affects the results with low decay rates, which correspond to those cases with small values of absorption coefficient. Compared with Figure 10(a), there is less variation between results for different values of scattering coefficient and the results are more consistent with the corridor model of Eq. (2).

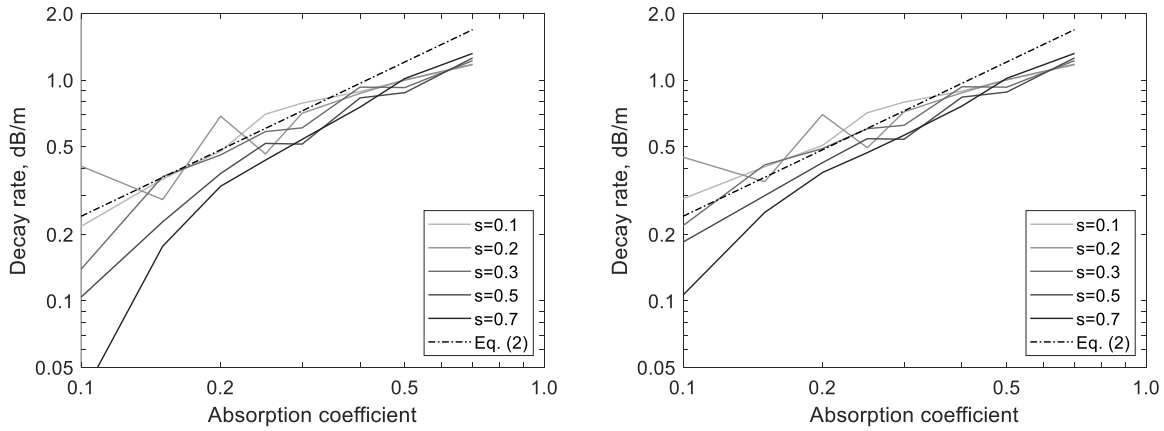

Figure 10. Decay rate Δ obtained from ray tracing models: (a) without correcting for end reflections; (b) after correcting for end reflections. Results obtained for range 2 to 9 m from the source.

From the measurements, it was found in Figure 5 that plotting the decay rates against reverberation time gave a consistent trend. However, from the results of the ray tracing model this is no longer the case, as shown in Figure 11. For low values of scattering coefficient, the results are close to the measurement trend line, whereas for high values of scattering coefficient they are lower, by up to a factor of 5. Although the evidence is rather indirect, these results suggest that, to model a vehicle interior, a relatively low scattering coefficient is more appropriate.

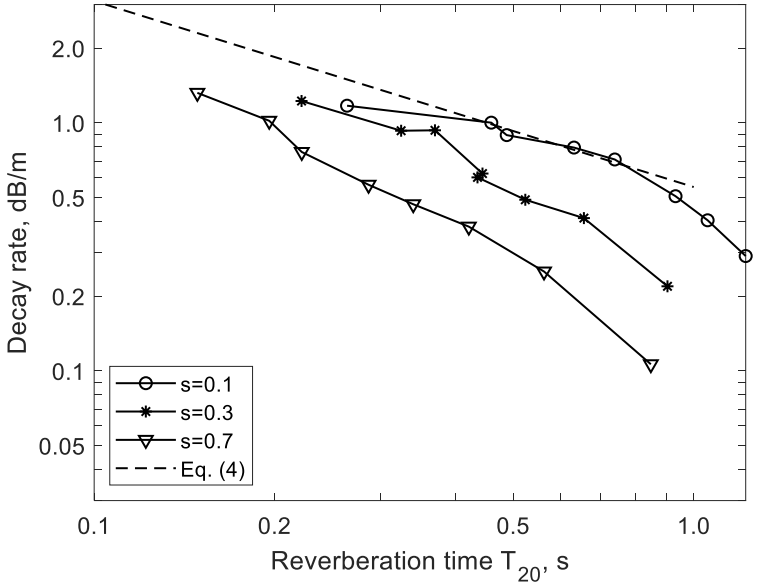

Figure 11. Decay rate Δ obtained from ray tracing models for range 2 to 9 m from the source for different values of scattering coefficient after correcting for end reflections, plotted against reverberation time T_{20}. Also shown is the trend line from the measurements in Figure 5 (Eq. (4)).

4. Estimating absorption and decay rate from measured reverberation time

In practice, the acoustic properties of a rail vehicle are usually assessed using measurements of reverberation time. The spatial decay is rarely measured and the absorption coefficients of the interior surfaces are often unknown. Although the experimental results gave a consistent trend of decay rate against reverberation time, Eq. (4), there is no direct theoretical justification for this expression. Moreover, as the absorption present in the experiments is unknown, in order to make comparisons with the various theoretical results it is necessary to derive the average absorption coefficient from either the reverberation time or the decay rate.

Additionally, the degree of scattering is also unknown, making direct comparisons with the ray tracing model problematic.

It is possible to derive the average absorption coefficient from the reverberation time by using Eq. (7) based on the mean free path length given by Picaut et al. [20]. To assess this approach, the decay rate has then been determined by using this absorption coefficient in the analytical expression, Eq. (2). This expression has been seen to be reasonably consistent with the ray tracing results (for which the absorption coefficient is known) after removal of the direct field and the end reflections (Figure 10(b)). For the measurements, the decay rate results based on the absorption obtained from Eq. (7) are compared with the measured decay rates in Figure 12(a). If the absorption is derived from the Sabine formula, the decay rates (not shown here) are around a factor of 2 smaller and therefore agree less well with the measurements.

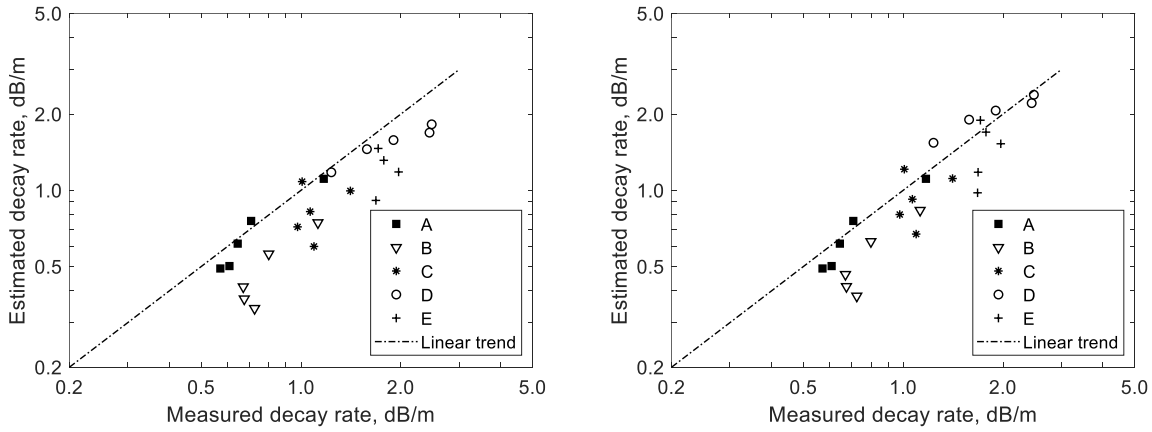

(a) (b)

Figure 12. Decay rate Δ estimated from measured reverberation times by using Eq. (7) to determine average absorption and Eq. (2) to relate this to the decay rate. (a) Based on full cross-section; (b) based on reduced cross-section allowing for the area of the seats.

The agreement can be improved further by considering that the effective cross-section of the carriage is reduced by the presence of the seating; free propagation therefore only occurs in the region above the seat backs. To allow for this, the height of the carriage used in determining U, S and S_{2D} has been reduced by 0.6 m for vehicles B and C and by 0.8 m for vehicles D and E which had taller seats. This change in height has only a small effect on the estimate of absorption coefficient using Eq. (7) but it modifies the resulting decay rate,

particularly for vehicles D and E. The results are shown in Figure 12(b) and indicate that more consistent estimates of decay rate have been obtained.

So, in summary, for railway carriages it appears that the average absorption coefficient is more reliably obtained from the reverberation time by using the formula given by Picaut et al. [20] for the mean free path length (i.e. using Eq. (7)) rather than by using the conventional Sabine formula. This approach gives results that are consistent with the measured decay rate, provided that a reduced cross-section area is used in Eq. (2) to allow for the blocking effect of the seating. It is applicable to vehicles with either open gangways or high levels of absorption, in which end reflections have negligible contribution to the sound field; it is less suited to situations in which there are separating walls between different compartments, such as analysed in [7].

5. Suitability of statistical energy analysis for train interior acoustics

5.1 Formulation

Statistical energy analysis (SEA) is also commonly used for modelling the interior of trains [10-14] and is simpler to apply than ray tracing, requiring less geometrical detail and fewer input parameters. SEA is typically used as a method to determine the transmission of noise and vibration from sources outside the carriage; the modelling of the interior sound field then becomes a part of such a model, e.g. [10, 12-14, 22]. In SEA, the system is divided into subsystems which can be both structural and acoustic, although here only acoustic subsystems are considered.

The SEA method is based on the power balance equation for each subsystem [21]

$$\omega\eta_i E_i + \sum_{j=1, j\neq i}^{n} \omega\eta_{ij} E_i - \sum_{j=1, j\neq i}^{n} \omega\eta_{ji} E_j = P_{\mathrm{in},i}, \quad i = 1,2,3, \ldots \tag{8}$$

where $P_{\mathrm{in},i}$ is the power input to subsystem i, E_i is the energy in subsystem i, ω is the angular frequency, η_{ij} are coupling loss factors (CLF) between subsystems i and j ($i \neq j$) and η_i is the dissipation loss factor of subsystem i. SEA relies amongst other things on the assumption of weak coupling, which requires $\eta_{ij} \ll \eta_i$.

For acoustic subsystems, the dissipation loss factor is related to the absorption coefficient by [21]

$$\eta_i = \frac{c_0 S_i \alpha_i}{4\omega V_i} \tag{9}$$

where c_0 is the speed of sound, S_i is the total surface area of the subsystem, V_i is its volume and α_i is its average absorption coefficient. Similarly, the coupling loss factor from subsystem i to subsystem j is given by

$$\eta_{ij} = \frac{c_0 S_{ij} \tau_{ij}}{4\omega V_i} \tag{10}$$

where $S_{ij} = S_{ji}$ is the area of the interface between the cavities and τ_{ij} is the transmission coefficient of this interface. For subsystems within a large acoustic enclosure, it is natural to set $\tau_{ij} = 1$. Unfortunately, the weak coupling condition is generally not met in such a situation and the behaviour may be more global rather than local to each subsystem.

Eq. (8) can be solved to determine the stored energy in each subsystem. The average sound pressure levels in a subsystem can be obtained from the stored energy E_i as [28]:

$$L_{p,i} = 10\log_{10}\left(\frac{\rho c_0^2 E_i}{V_i {p_{\mathrm{ref}}}^2}\right) \tag{11}$$

where p_{ref} is the reference sound pressure, 2×10^{-5} Pa.

5.2 Division into subsystems

In conventional SEA, the division of an acoustic cavity into arbitrary subsystems is potentially problematic, especially for a long enclosure such as a train interior. As an example, results are presented for an acoustic cavity of length 20 m that is subdivided into different numbers of subsystems. The cross-section has dimensions 2.1×2.5 m, identical to the ray tracing model in Section 3. A single source with a sound power level of 105 dB re 10^{-12} W is introduced in the subsystem at the left-hand end. Results are presented in Figure 13 for average absorption coefficients of 0.1 and 0.3 and a frequency of 1 kHz (although in this form the results are independent of frequency). The sound decay increases as the number of subsystems increases. Thus, the rate of decay depends on the way in which the system is subdivided and it does not converge as the model is refined.

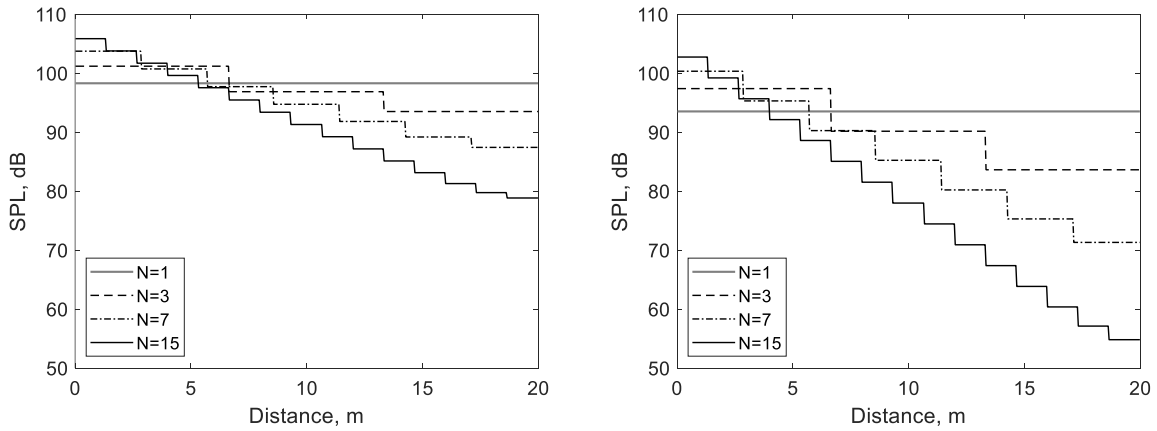

Figure 13. Sound pressure level in a carriage predicted using SEA model with different numbers of subsystems (*N*): (a) α = 0.1; (b) α = 0.3.

To illustrate this further, the decay rate with distance (in dB/m) from conventional SEA models has been calculated using different models, with absorption coefficients of 0.1, 0.2, 0.3, 0.5, 0.7 or 1.0. Each model has 50 subsystems of equal lengths (1, 2, 4, 8 or 16 m), so that the overall length of the model varies. This number of subsystems is chosen here to represent a semi-infinite model with no effect from end reflections and is not intended to be representative of a train. The cross-section again has dimensions 2.1×2.5 m. Figure 14 shows the decay with distance obtained from these SEA models (obtained between the levels in the first and the 11th subsystem divided by the distance between their centres), normalised by the decay obtained from Eq. (2), for this range of parameters. These results are plotted against the ratio η_i/η_{ij} from the SEA model, which from Eqs (9) and (10), can also be expressed as

$$\frac{\eta_i}{\eta_{ij}} = \frac{S_i\alpha_i}{S_{ij}\tau_{ij}} = \frac{U\alpha L_i}{S_{2D}} \tag{12}$$

where S_i is the area of the sides, top and bottom of the subsystem, α_i is its average absorption coefficient, $S_{ij} = S_{2D}$ is the cross-section area between adjacent subsystems and U is the perimeter length of the cross-section. L_i is the length of the subsystem. Expressed in this form the results collapse to a single line; although not shown here, they are found also to be independent of the cross-section of the model (i.e. S_{2D} and U).

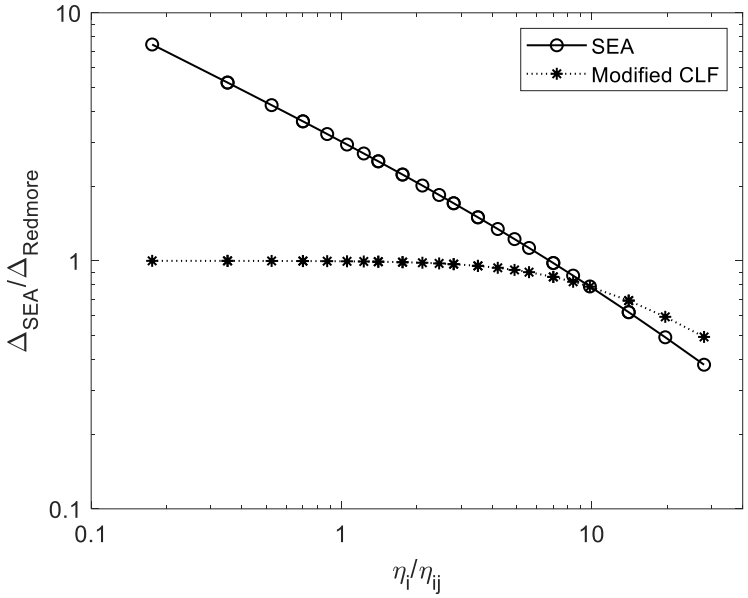

Figure 14. Ratio of sound decay rate obtained from SEA models to that predicted by Eq. (2), plotted against ratio η_i/η_{ij}.

Typical values used to represent a rail vehicle interior are average absorption coefficients in the range 0.1-0.3 and subsystem lengths 2-4 m, giving values of η_i/η_{ij} between about 0.3 and 2. From Figure 14, this indicates that, for such typical parameters, a conventional SEA model will give a decay with distance that is too large compared with Eq. (2). Reducing the length of the subsystems will increase this decay rate further, whereas for very long subsystems or much higher absorption the decay rate from the SEA model will become too low. Importantly, as seen above, the results from the SEA model do not converge when varying the length of the subsystems. Note also that the 'weak coupling' condition corresponds to $\eta_i/\eta_{ij} \gg 1$ which is mostly not satisfied for realistic parameter values.

5.3 Modified CLF

Based on the analytical model of Redmore and Flockton [17], Craik [21] derived an equivalent CLF for use in an SEA model of a corridor, in which it is assumed that all subsystems have the same length and the same absorption:

$$\hat{\eta}_{ij} = \frac{100 c_0 A_i}{4(\ln 10)^2 \omega S_{ij} L_i^3 \Delta^2} \tag{13}$$

where L_i is the length of the subsystem, $S_{ij} = S_{2D}$ is its cross-section area and $A_i = U L_i \alpha$ is its absorption area. Substituting for Δ from the revised form, Eq. (2), this gives

$$\hat{\eta}_{ij} = \frac{c_0 \pi^2 S_{2D}}{4\omega L_i^2 U \alpha} \tag{14}$$

Replacing the coupling loss factor by this modified one, the decay rate obtained from the SEA model should match that predicted by Eq. (2) on which it is based. The decay rate from this modified SEA model is also shown in Figure 14, again normalised by the decay rate obtained from Eq. (2) and plotted against the ratio η_i/η_{ij} (based on the original value of η_{ij}, i.e. Eq. (12)). There is good agreement for values of η_i/η_{ij} less than about 5, for which the result is within 10% of the decay rate from Eq. (2), but for higher values the SEA model predicts a lower decay rate than Eq. (2) due to an approximation in the derivation given in [21].

In Section 4 a method to determine the average absorption coefficient from the reverberation time was presented. As shown in Figure 12(b) this approach gives results that are consistent with measured decay rates. The resulting absorption coefficients can finally be used in an SEA model with the modified CLFs of Eq. (14), giving a model with the same decay rate and providing a practical modelling approach for a railway vehicle interior.

6. Conclusions

The reverberation time and spatial decay of sound have been measured in five diverse train interiors using an omnidirectional sound source. The measured sound pressure level follows a fairly linear dependence on longitudinal distance and the rate of decay obtained from this fits a consistent trend against reverberation time over all five datasets.

A ray tracing model in CATT-Acoustic with simplified geometry has been used to investigate the dependence of spatial decay and reverberation time on the absorption and scattering coefficients. Removing the direct sound field causes the decay curves to become closer to linear, apart from cases with high absorption and low scattering. The results from these simulations show that the reverberation time depends strongly on the degree of scattering; for high values of scattering coefficient the reverberation time approaches the Sabine estimate whereas for low values it can exceed the Sabine estimate by up to a factor of 2.5. This illustrates the difficulty in deducing average absorption coefficients from the measured

reverberation times. The spatial decay rates obtained from the ray tracing model are mostly lower than those obtained from the measurements for a given reverberation time, with the results also depending strongly on the degree of scattering. More consistent results are obtained from the ray tracing results when the effect of end reflections is removed but this is not necessary for the measurement results as the trains either had open gangways with no interior doors between carriages or had a large decay rate.

For typical parameter values, it is demonstrated that a conventional SEA approach will overestimate the spatial sound decay in a rail vehicle for typical parameter values. Moreover, the spatial decay from such an SEA model depends explicitly on the length of the subsystems used and does not converge as the number of subsystems within a certain length is increased or decreased. To overcome this, the modified coupling loss factor proposed by Craik [21] can be used in SEA models and this gives good agreement with the analytical corridor model of Redmore and Flockton [17] on which it is based, at least for parameters typical of train interiors.

A practical way to deal with these difficulties is proposed, in which the average absorption can be estimated from the reverberation time by using a modified expression for the mean free path length from Picaut et al. [20]. The decay rate is then found to be consistent with the analytical corridor model when using this absorption coefficient and using a reduced cross-section area to allow for the blockage caused by the seats. This average absorption can finally be used in the modified SEA model. The proposed approach can be used for vehicles in which end reflections have negligible contribution to the sound field (vehicles with either open gangways or high levels of absorption); it is less suited to situations in which there are separating walls between different compartments.

Acknowledgements

This work was supported by the Shanghai Sailing Program [No. 20YF1451100], the Natural Science Foundation of Shanghai [No. 21ZR1467100] and sponsored by Shanghai Collaborative Innovation Research Center for Multi-network & Multi-modal Rail Transit. All data published in this paper are openly available from the University of Southampton repository at: https://doi.org/10.5258/SOTON/D2398.

References

1 Thompson D. Railway Noise and Vibration: Mechanisms, Modelling and Means of Control. Oxford: Elsevier; 2008.

2 Bouvet P, Rissmann M. Industrial methodologies for the prediction of interior noise inside railway vehicles: airborne and structure-borne transmission. In: Degrande G. et al., editors. Proceedings of 13th International Workshop on Railway Noise, Ghent, Belgium, 16-20 September 2019, Notes on Numerical Fluid Mechanics and Multidisciplinary Design. 2021;150:41-54.

3 Zhang J, Xiao XB, Sheng XZ, Fu R, Yao D, Jin XS. Characteristics of interior noise of a Chinese high-speed train under a variety of conditions. J Zhejiang Univ-Sci A (Appl Phys & Eng) 2017:18;617-630.

4 Bracciali A, Pellegrini C, FEM analysis of the internal acoustics of a railway vehicle and its improvements. World Congress on Railway Research, Florence, Italy, Nov. 1997.

5 Wu D, Ge J. Modelling the interior sound field of a railway vehicle using Finite Element method. Acoustics Australia 2014:42;211-212.

6 Létourneux F, Guerrand S, Poisson F. Low-frequency acoustic transmission of high-speed trains: simplified vibroacoustic model. Journal of Sound and Vibration 2000:231;847-851.

7 Forssén J, Tober S, Corakci AC, Frid A, Kropp W. Modelling the interior sound field of a railway vehicle using statistical energy analysis. Applied Acoustics 2012:73;307-311.

8 Panahi E, Younesian D. Acoustic performance enhancement in a railway passenger carriage using hybrid ray-tracing and image-source method. Applied Acoustics 2020:170;107527.

9 Yoshizawa T, Mochida T, Yamazaki T. Study of analysis method of interior noise in railway cars by means of ray tracing method, Bulletin of the JSME, Mechanical Engineering Journal 2019:6(5);18-00449.

10 Sadri M, Brunskog J, Younesian D, Application of a Bayesian algorithm for the Statistical Energy model updating of a railway coach, Applied Acoustics 2016:112;84-107.

11 Li H, Thompson D, Squicciarini G, Liu X, Rissmann M, Bouvet P, Denia FD, Baeza L, Martín Jarillo J, Moreno García-Loygorri J, A framework to predict the airborne

noise inside railway vehicles with application to rolling noise, Applied Acoustics 2021:179;108064.

12 Zheng X, Hao Z, Wang X, Mao J, A full-spectrum analysis of high-speed train interior noise under multi-physical-field coupling excitations, Mechanical Systems and Signal Processing 2016:75;525-543.

13 Dai W, Zheng X, Luo L, Hao Z, Qiu Y, Prediction of high-speed train full-spectrum interior noise using statistical vibration and acoustic energy flow, Applied Acoustics 2019:145;205-219.

14 Zhang J, Xiao X, Sheng X, Zhang C, Wang R, Jin X, SEA and contribution analysis for interior noise of a high-speed train, Applied Acoustics 2016:112;1158-1170.

15 Fahy F, A note on the subdivision of a volume of air in a vehicle enclosure into SEA subsystems, Journal of Sound Vibration 2004:271;1170-1174.

16 Kang J, Sound attenuation in long enclosures, Building and Environment 1996:31;245–253.

17 Redmore T, Flockton S. A design formula for predicting the attenuation of sound along a long corridor, Acoustic Letters 1977:1;21-24.

18 Redmore TL, A method to predict the transmission of sound through corridors, Applied Acoustics 1982:15;133-146.

19 Hopkins C, Sound Insulation, Amsterdam: Butterworth-Heinemann, pp62-65.

20 Picaut J, Simon L, Polack JD, Sound field in long rooms with diffusely reflecting boundaries. Applied Acoustics 1999:56;217-240.

21 Craik RJM, Sound Transmission through Buildings using Statistical Energy Analysis, Aldershot: Gower Publishing Limited, 1996.

22 Orrenius U, Enblom R, Acoustic optimization of car-body structures: Weight efficient setting of subsystem requirements, Proceedings Inter-noise, Den Haag, Netherlands, 2001.

23 Kohrs T, Kirchner KR, Brick H, Fast D, Guiral A, Industrial engineering framework for railway interior noise predictions, in G. Degrande, et al. (Eds) Proceedings of 13th International Workshop on Railway Noise, Ghent, Belgium, 16-20 September 2019, Notes on Numerical Fluid Mechanics and Multidisciplinary Design 150 (2021) 158–166.

24 Jang H, Hopkins C, Prediction of sound transmission in long spaces using ray tracing and experimental Statistical Energy Analysis, Applied Acoustics 2018:130;15-33.

25 ISO 3382-2:2008 Acoustics – Measurement of room acoustic parameters – Part 2: Reverberation time in ordinary rooms. International Standardisation Organisation, Geneva, 2008.

26 CATT-Acoustic, https://www.catt.se/CATT-Acoustic.htm

27 Pujolle J, Les différentes définitions du libre parcours moyen du son dans une salle (The different definitions of mean free path length of sound in a room). Revue d'Acoustique 1976:36;44-50.

28 Thompson D, Nelson P, Fundamentals of acoustics, in Fahy F, Thompson D, editors, Fundamentals of Sound and Vibration, second edition, Boca Raton: CRC Press, 2015.